Available online at www.sciencedirect.com
ScienceDirect
Magnetic Resonance Imaging 27 (2009) 1096–1103
MAGNETIC RESONANCE IMAGING

Reproducibility of myelin water fraction analysis: a comparison of region of interest and voxel-based analysis methods

Sandra M. Meyers[a], Cornelia Laule[b], Irene M. Vavasour[b], Shannon H. Kolind[c], Burkhard Mädler[c,d], Roger Tam[b], Anthony L. Traboulsee[e], Jimmy Lee[e], David K.B. Li[b], Alex L. MacKay[b,c,*]

[a]Department of Physics, University of Alberta, Edmonton, Canada T6G 2G7
[b]Department of Radiology, University of British Columbia, Vancouver, Canada V6T 2B5
[c]Department of Physics & Astronomy, University of British Columbia, Vancouver, Canada V6T 1Z1
[d]Philips Healthcare, Vancouver, Canada V6T 2B5
[e]Department of Medicine, University of British Columbia, Vancouver, Canada V6T 2B5

Received 18 October 2008; revised 30 January 2009; accepted 19 February 2009

Abstract

This study compared region of interest (ROI) and voxel-based analysis (VBA) methods to determine the optimal method of myelin water fraction (MWF) analysis. Twenty healthy controls were scanned twice using a multi-echo T_2 relaxation sequence and ROIs were drawn in white and grey matter. MWF was defined as the fractional signal from 15 to 40 ms in the T_2 distribution. For ROI analysis, the mean intensity of voxels within an ROI was fit using non-negative least squares. For VBA, MWF was obtained for each voxel and the mean and median values within an ROI were calculated. There was a slightly higher correlation between Scan 1 and 2 for the VBA method (R^2=0.98) relative to the ROI method (R^2=0.95), and the VBA mean square difference between scans was 300% lower, indicating VBA was the most consistent between scans. For the VBA method, mean MWF was found to be more reproducible than median MWF. As the VBA method is more reproducible and gives more options for visualization and analysis of MWF, it is recommended over the ROI method of MWF analysis.

Keywords: Myelin water; T_2 relaxation; NNLS; White matter; Voxel-based analysis

1. Introduction

The proton signal from central nervous system tissue during a conventional magnetic resonance (MR) exam is almost entirely due to water. Different water environments in brain can be probed by measuring T_2 relaxation. Previous studies involving T_2 relaxation have shown that MRI signal from water in healthy human brain is generated from three different components: a long T_2 component (~2 s) arising from cerebrospinal fluid (CSF), an intermediate component (~80 ms) attributed to intra- and extracellular water, and a short T_2 component (~20 ms) thought to be due to water located between the myelin bilayers (myelin water) [1–3]. The ratio of the short T_2 signal (myelin water) to the total signal (total water content) gives the myelin water fraction (MWF) [4], which has been shown to correlate strongly with histological staining for myelin [5–8]. In recent years, a number of groups have conducted research in the area of T_2 relaxation in both brain and spinal cord, with particular interest in studying MWF in healthy controls and diseases such as multiple sclerosis, schizophrenia, phenylketonuria and Alzheimer's disease [1,9–16].

The first step in a T_2 relaxation experiment is the acquisition of T_2 decay curves. The most common approach is to collect multiple echoes in a single MR sequence. Many investigators have used the Poon-Henkelman multiple spin-echo imaging sequence [17]. While this sequence is proven to yield robust T_2 decay curves, it suffers from the disadvantage of being a single slice technique. A more

* Corresponding author. Department of Radiology, University of British Columbia Hospital, Vancouver BC, Canada, V6T 2B5. Tel.: +1 604 822 7890; fax: +1 604 827 3339.
E-mail address: mackay@physics.ubc.ca (A.L. MacKay).

0730-725X/$ – see front matter © 2009 Elsevier Inc. All rights reserved.
doi:10.1016/j.mri.2009.02.001

practical approach to collecting T_2 decay curves was recently applied by Oh et al. [11], who employed a novel spiral acquisition technique [18,19] which collected images at 12 echo times (TE) for 16 slices in 10 min. Mädler et al. [20] developed a 3D multiecho pulse sequence (used here) which is capable of collecting 32 echoes from seven slices in less than 20 min.

While there are several different methods available to analyse in vivo multiexponential decay data [21–24], the method most frequently applied in the literature is the nonnegative least squares (NNLS) algorithm [6,19,25–28]. The NNLS approach, which uses a χ^2 minimization algorithm to fit the decay curve with a T_2 distribution (i.e., a plot of amplitude vs. T_2 time), assumes a large number of T_2 times and solves for the corresponding zero or non-zero amplitudes; it thereby does not involve a priori assumptions as to the number of contributing exponentials. From the T_2 distribution, the MWF can be determined as the fractional signal with T_2 between 15 and 40 ms [28].

Using NNLS, several methods can be employed to determine MWF for a defined region in an image. A common approach (labelled herein as the "ROI" method) is to outline a region of interest (ROI) on an image from one echo of the T_2 relaxation data and then calculate a single decay curve using the average of the signal intensity from all the voxels within this ROI for each echo. This average ROI decay curve is then inverted to a single T_2 distribution using NNLS. A second approach is to carry out the NNLS inversion using voxel based analysis (VBA). In this method (labelled the "VBA" method), the MWF is first determined for every voxel in the image in order to create a "myelin water map." ROIs are then applied to the myelin water map, and the mean or median MWF of contributing voxels within the ROI is calculated. If NNLS was a linear inversion technique, MWF values from the ROI and VBA analysis approaches defined above would be identical for the same region; however, NNLS is a complex algorithm that produces T_2 distributions which are sensitive to noise. Since the two approaches sample the noise differently, we expect the resulting MWF values to differ slightly.

Each method has its strengths and weaknesses. The ROI technique gives a decay curve with an improved signal-to-noise ratio (SNR) and is therefore used more often. It is also less computationally intensive, thereby taking less time to conduct the analysis. The VBA method for calculating MWF in an ROI is more flexible in that it offers more options for analysis, including determination of both mean and median MWF, as well as MWF histograms. The VBA method also gives a more traditional measure of error, such as the standard deviation within a region of interest, which is not available with the ROI method.

The ultimate goal of this study was to determine the optimal method of MWF analysis using NNLS. Specifically, we wished to determine which of the above defined ROI and VBA analysis techniques had the smallest variability in repeated brain MWF measurements from 20 healthy controls using a 3D acquisition technique [20]. Subjects were scanned twice and MWF was compared between scans in order to investigate reproducibility. With the VBA method, results employing the mean MWF were compared to those using the median MWF.

2. Methods

2.1. Subject information

Twenty healthy volunteers (11 females, 9 males), mean age 30.1 years (range from 21 to 49 years), with no known neurological disorders or MR-visible brain abnormalities were scanned twice (labelled Scan 1 and Scan 2) in 1 day. On average, the time between scans was 2.5 h (range: 1.5–3.75 h). This study was approved by our institution's ethical review board. Written, informed consent was obtained from all subjects.

2.2. MRI experiments

All MR examinations were conducted using a six-element phased-array head coil on a 3.0-T MR scanner (Achieva 3.0T, Philips Medical Systems, Best, The Netherlands). After a sagittal localizer and an inversion recovery (IR) experiment [5 TIs (150–3000 ms), TR/TE=6.4/3.1 ms, SENSE=2, TFE=120, shot interval=5000 ms, FA=10°, 13 slices, 256×256 matrix] [29], a 3D 32 echo sequence for T_2 relaxation measurement was acquired (TR=1200 ms, echo spacing=10 ms, SENSE=1, 7 slices, 256×128 matrix, axial orientation, acquisition time=19 min) [20]. The field of view for all experiments was 240×205 mm, and slice thickness was 5 mm.

2.3. Regions of interest

Five grey matter (GM) (thalamus, head of the caudate nucleus, cortical grey, cingulate gyrus, putamen) and five white matter (WM) (genu of the corpus callosum, major forceps, minor forceps, posterior internal capsules, splenium of the corpus callosum) structures were outlined on the Scan 1 IR 150-ms MR image (chosen for best contrast between grey and white matter) on a transverse slice through the base of the genu and splenium of the corpus callosum. These ROIs were then mapped onto Scan 1 and Scan 2 of the multi-echo T_2 experiment, which were registered to the baseline IR 1500 ms T_1 image using in-house registration software based on the maximization of mutual information [30]. The registration method was a multiscale technique that used the Shannon entropy computed from the joint histogram of the two images as the similarity measure. Image interpolation was performed using a Blackman windowed sinc filter.

2.4. T_2 Decay Curve Analysis

The decay curves were assumed to be multi-exponential in nature. A general equation which can be used to

describe the measured multiexponential relaxation signal, y_i , is [28]:

$$y_i = \sum_{j=1}^{M} S_j \exp\left(-t_i/T_{2j}\right), \quad i = 1, 2, \ldots, N$$

where t_i are the measured times in the decay curves, M=120 is the number of logarithmically spaced T_2 times within the range of 15 ms to 2s, N=32 is the total number of data points and s_j is the relative amplitude for each partitioned T_2 time. An NNLS algorithm was used to minimize both χ^2 and an energy constraint that smoothes the T_2 distribution, $s_j(T_{2j})$, providing more consistent fits in the presence of noise [26,28,31]. The following expression was minimized:

$$\chi^2 + \mu \sum_{j=1}^{M} s_j^2, \mu \geq 0$$

The larger the μ parameter, the more the above routine smoothes the T_2 distribution at the cost of misfit. For the case of μ=0, χ^2_{min} would result and the T_2 distribution would consist of discrete spikes. Regularized smooth T_2 distributions were created by minimizing the above expression with the energy constraint of $1.02\chi^2_{min} \leq \chi^2 \leq 1.025\chi^2_{min}$.

2.5. Myelin water fraction and SNR_{NNLS} calculation

MWF was defined as the sum of the amplitudes s_j with T_2 relaxation times between 15 and 40 ms relative to the total sum of the amplitudes s_j in the T_2 distribution, and was expressed as a percentage. For the ROI based analysis, a single decay curve derived from the average intensity within an ROI for each echo was fit using NNLS. For VBA, decay curves were generated for each individual voxel in the entire ROI and myelin water maps were created by displaying the MWF at each voxel in the image. ROIs were then mapped to the myelin water maps and both the mean and median MWF were determined from the contributing voxels within that ROI. A measure of signal to noise for the decay curve, SNR_{NNLS}, was calculated as the ratio of the signal amplitude at TE=0 ms of the decay curve to the standard deviation of the residuals from the NNLS fit [32].

2.6. Statistical analysis

Linear regression and Pearson correlations were calculated for VBA MWF vs. ROI MWF for each of the 20 subjects for each scan, and then averaged. A two-tailed paired Student's t test was used to compare the mean MWF of one structure for the VBA method with that of the ROI method, and to compare the mean SNR_{NNLS} of the two methods (including data for all 20 subjects). Statistical significance was taken as $P \leq .05$. A Bland-Altman plot was created using the difference between and mean of VBA and ROI MWFs [33]. The Bland-Altman plot is used to show the level of agreement between two methods measuring the same parameter (in this case, VBA and ROI measuring MWF).

To test reproducibility, linear regression was performed and Pearson correlation coefficients were calculated between Scan 1 and Scan 2 for each subject, for each analysis method. These measurements were then averaged between all twenty subjects for each analysis method. A two-tailed paired Student's t test was used to compare MWF between scans; this was conducted once for each method on all subjects' data on a per structure basis. The mean square difference between Scan 1 and Scan 2 MWF was calculated (including all subjects' data).

Finally, mean and median MWF values were compared for correlation and reproducibility between Scan 1 and Scan 2.

3. Results

3.1. Comparisons within a single scan

Table 1 lists the MWF values obtained for all 10 structures using the ROI and VBA approaches. Student's t-tests revealed that MWF was significantly higher when using the VBA method, compared to the ROI method, for all structures except for the minor forceps and thalamus. SNR_{NNLS} was found to be significantly higher for the ROI method relative to the VBA method for all structures except the cingulate gyrus (See Table 2).

3.2. Correlations between ROI and VBA

For each subject, strong correlations were observed between VBA and ROI MWFs. The average R was 0.97 (range: 0.95–0.98), the slope of the linear regression was close to 1 (average 1.02, range 0.91–1.15), and the mean intercept was 0.86% (-0.04%–1.67%). Fig. 1 shows the

Table 1
MWF measurements for ROI and VBA methods for Scan 1

	ROI MWF (%)	VBA MWF (%)
Grey matter		
Caudate	1.5±0.2	2.1±0.1*
Cingulate gyrus	0.00±0.00	0.70±0.09*
Cortical grey	0.01±0.00	0.60±0.05*
Putamen	2.9±0.3	4.3 ±0.2*
Thalamus	3.5±0.2	3.5±0.2
Average	1.6±0.1	2.23±0.09*
White matter		
Genu	8.6±0.3	10.2±0.2*
Posterior internal capsules	15.4±0.3	17.2±0.2*
Major forceps	6.9±0.2	7.4±0.2*
Minor forceps	3.9±0.2	3.7±0.2
Splenium	12.5±0.3	14.4±0.2*
Average	9.5±0.2	10.6±0.3*

MWF (%) values were averaged for ROIs drawn by one observer over all twenty subjects. Means are shown, together with the standard error.

* Populations were considered significantly different if $P \leq .05$.

Table 2
SNR_{NNLS} Measurements for ROI and VBA methods for Scan 1

	ROI SNR_{NNLS}	VBA SNR_{NNLS}
Grey matter		
Caudate	720±40	280±9**
Cingulate gyrus	300±40	240±10
Cortical grey	150±7	160±6**
Putamen	850±40	330±8**
Thalamus	550±40	250±7**
Average	510±20	250±5**
White matter		
Genu	1100±70	400±9**
Posterior internal capsules	750±40	320±8**
Major forceps	500±40	300±10**
Minor forceps	410±60	310±20*
Splenium	600±40	270±6**
Average	660±30	320±6**

SNR_{NNLS} values were averaged for ROIs drawn by one observer over all twenty subjects. Means are shown, together with the standard error. Populations were considered significantly different if $P \leq .05$.

* $P \leq .05$.

** $P \leq .0001$.

comparison of the VBA method to ROI analysis for all subjects for Scan 1. Fig. 2 is a Bland–Altman plot for the VBA and ROI methods of estimating MWF. There was a small positive VBA bias which fitted the equation: bias=0.043∗(MWF(VBA)+MWF(ROI))/2+0.006. The steep slope at the origin of the Bland–Altman plot arises from regions where the ROI method returned a zero MWF.

3.3. Comparisons between scans

Fig. 3 displays the correlations between MWF values on repeated scans for both analysis methods, for all regions from all subjects combined. While both approaches gave MWF values that were highly correlated between scans [ROI method: mean R=0.95 (0.87–0.99), VBA method: mean R=0.98 (0.88–1.00)], when compared to the ROI technique, the correlation for the VBA method was 3.4% higher (range −5.8% to 10.0%). Linear regression of Scan 1 vs. Scan 2 for the ROI method gave a mean slope of 1.02 (0.81–1.12) and a mean intercept of 0.15% (–0.70% to 1.32%). The VBA regression had a mean slope of 1.02 (0.91–1.15) and mean intercept of 0.02% (–0.46% to 0.73%). The mean square difference between Scan 1 and Scan 2 was 3.84 for the ROI method and 1.30 for the VBA method. t Tests showed that, in general, MWF did not significantly differ between scans for either method.

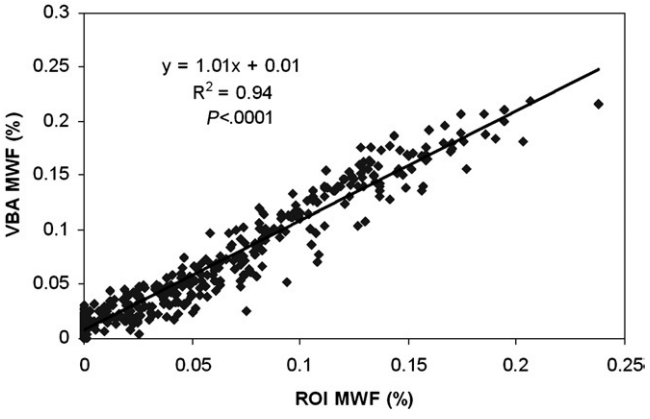

Fig. 1. Plot of MWF values obtained by the VBA method vs. MWF obtained by the ROI method, including all subjects' data for Scan 1.

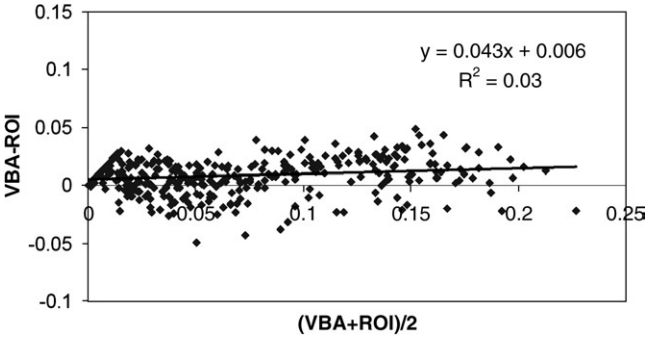

Fig. 2. Bland–Altman plot with the difference between VBA and ROI MWF plotted against the mean of the two methods for Scan 1.

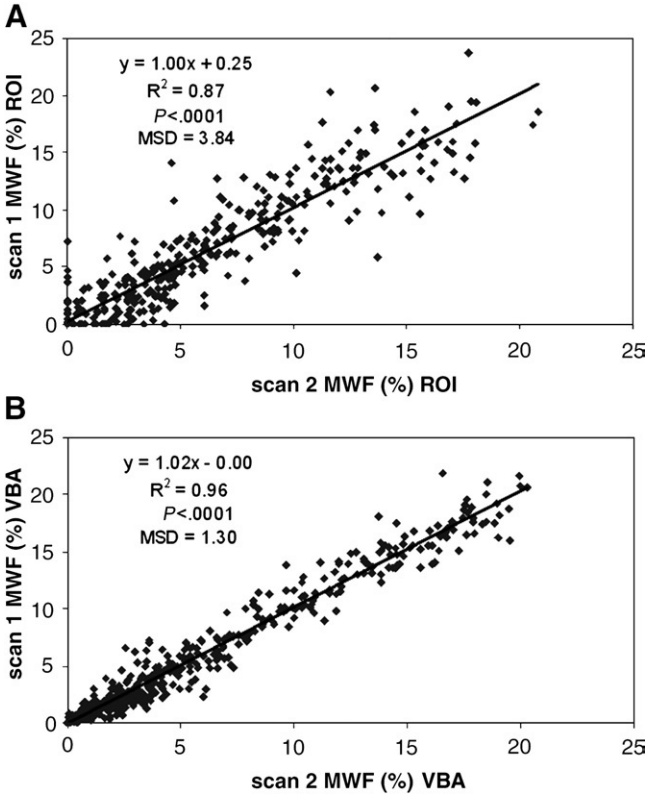

Fig. 3. Plot of MWF values obtained in Scan 2 compared to those obtained in Scan 1, including all subjects' data. (A) Measurements acquired ROI analysis. (B) Measurements acquired by VBA. While both methods show a strong correlation, the MSD of VBA is smaller than that of the ROI method. MSD, mean square difference.

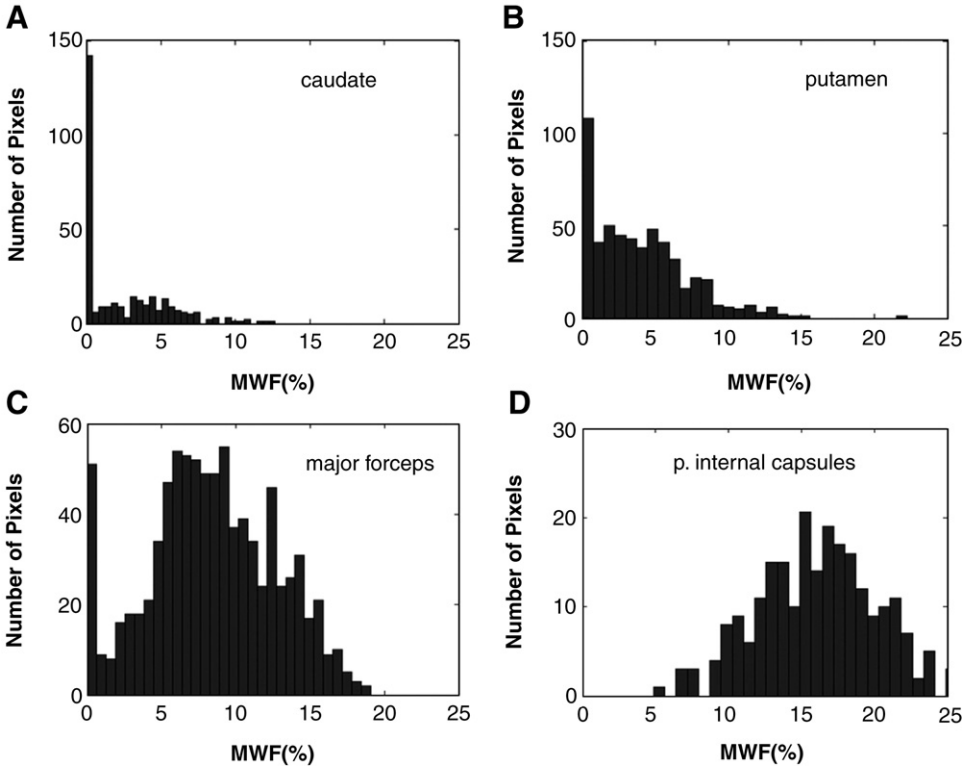

Fig. 4. Histograms of individual voxel MWF within single ROIs (left and right ROIs combined) for one subject. (A) shows a head of the caudate nucleus ROI (grey matter), (B) shows the putamen (grey matter), (C) shows the major forceps (white matter) and (D) shows the posterior interior capsules (white matter).

Also, neither scan had consistently higher mean MWF values than the other.

3.4. Comparison between the mean MWF and median MWF

Fig. 4 shows representative histograms of MWF for two GM and two WM structures. Generally, the distributions for WM structures were close to Gaussian in shape, while the distributions for GM structures were right skewed. The capability of examining the histogram of MWF voxels from a region is valuable because VBA gives the option of calculating other distribution parameters, for example the median MWF, which may be less susceptible to outlying data points.

The VBA median MWF is plotted vs. the mean MWF in Fig. 5. While the high correlation (R^2=0.99) showed that the two measurements were very similar, the median MWF had many more zero MWF values. Consequently, in all grey matter structures the median MWF was significantly lower than the mean MWF; however, in white matter the two statistics were similar. The mean square difference between Scan 1 and Scan 2 was 2.01 for the median MWF, compared to 1.30 for the mean MWF.

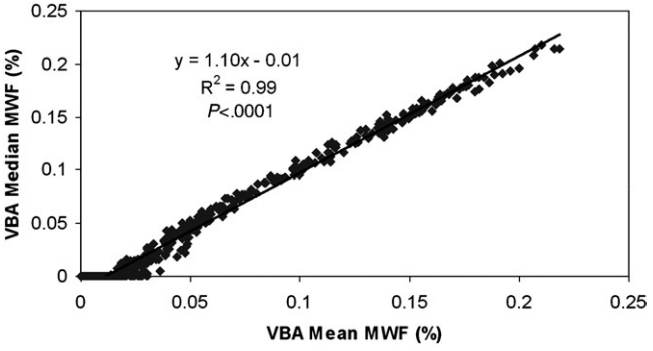

Fig. 5. Plot of VBA MWF values obtained from median of individual voxels within ROIs compared to those obtained from mean of individual voxels within ROIs, including all subjects' data for Scan 1.

4. Discussion

In this study, we determined that VBA MWF analysis was superior to ROI MWF analysis. VBA had the smallest variability in repeated MWF measurements in brain. Table 1 shows that MWF values obtained in this study for all analysis methods were approximately in agreement with results obtained by other studies at 1.5 and 3.0 T [4,11].

4.1. ROI and VBA results are correlated

While a few differences between the ROI and VBA analyses were observed, the consistently high correlation between the two methods, as well as the linear regression giving slopes of approximately 1.0 and intercepts close to zero, suggest strong similarity between the two analysis

methods. From the Bland–Altman plots and Table 1, it was clear that the VBA method generally returned significantly higher MWF values than the ROI method; however, the bias was relatively small (0.6–1.3 %) compared to the range of observed MWF (1.8–16.5 %). It is not clear to us why the VBA MWF values were higher in white matter. In many grey matter structures, e.g. caudate nucleus, the ROI method often returned zero; however, the VBA method averaged over a distribution of zero and positive MWF values (See Fig. 4), resulting in a non-zero mean MWF.

As stated previously, the VBA approach has an advantage over the ROI approach in that it enables the analysis of the distribution of MWF values in the designated region. Brain structure myelination is not necessarily uniform; this concept was exploited in a recent study of myelin development in the corpus callosum of young boys [34].

4.2. VBA showed highest reproducibility between scans

Although a high correlation and slope close to 1.0 (Fig. 3) were observed between MWF of Scan 1 and Scan 2 for both ROI and VBA methods, VBA gave the highest correlation. The VBA method also gave the lowest mean square difference between Scan 1 and Scan 2. These results suggest that VBA is the most reproducible analysis method.

Several previous studies have investigated reproducibility between scans and compared VBA and ROI analyses. A study by Galbraith et al. [35] which examined the reproducibility of dynamic contrast-enhanced MRI in muscle and tumours found that results for VBA and ROI analyses were similar. While analysis method did not dramatically affect reproducibility, VBA analysis gave slightly better reproducibility between scans in that study. This is consistent with our results. Figueiredo et al. [36] assessed the reproducibility of perfusion measurements using pulsed arterial spin labelling and found significantly higher perfusion values for VBA relative to ROI analysis. This was thought to be due to the wide range of transit times over large ROIs leading to underestimation by the ROI method, or the higher noise levels in VBA analysis leading to overestimation.

4.3. SNR_{NNLS} was highest for ROI method

ROI SNR_{NNLS} was significantly higher than VBA SNR_{NNLS} for all structures except the cingulate gyrus. However, the increase in SNR_{NNLS} for the ROI method was much less than one would have expected for noise which is normally distributed. There are three contributions to the residuals in the NNLS fit to the T_2 decay curve from multiecho imaging MR sequences: random noise, fluctuations due to physiological noise and flow artifact and systematic noise due to B_1 inhomogeneity. If the residuals were entirely due to random noise, the ratio of SNR_{NNLS} for the ROI method versus the VBA method would be expected to scale as the square root of the number of data points in the ROI. Since this ratio was (on average) about two and independent of ROI size, clearly signal averaging of random noise does not dominate SNR_{NNLS}. In regions of flow artifact, one expects even echo rephasing in multi-echo sequences; this explains why SNR_{NNLS} was similar for each analysis technique for the cingulate gyrus ROIs, which have contamination from CSF flow. Finally, in multiecho imaging sequences, there are generally oscillations in the first few echoes which occur when the refocusing pulse is not exactly 180° [37,38]. These oscillations are relatively similar in adjacent image voxels; hence, they are not removed by signal averaging. It is the presence of these oscillations which causes the ROI technique to have only about a factor of two better SNR_{NNLS} than the VBA technique. From our experience, using the current 3D T_2 acquisition and the same radiofrequency coil, structures with the highest radio frequency field homogeneity (the central region of brain) and presumably the closest to a 180° pulse, like the genu of the corpus callosum, gave rise to the highest SNR_{NNLS} for the ROI method; structures with a suboptimal B_1 field (more peripheral brain regions), like the minor forceps and cortical grey matter, gave rise to the lowest SNR_{NNLS} for the ROI method.

One advantage of the ROI technique over the VBA method is that it yields decay curves which have higher SNR. It is well known [19,26] that when the SNR drops below a threshold (approximately 100), there are inaccuracies with NNLS analysis. Fortunately, for the results presented here, the VBA method had a signal to noise ratio higher than 100. While the VBA technique is more time-consuming since it relies on the calculation of the computer intensive myelin water maps, these myelin water maps are useful because they give a visual presentation of MWF. The VBA method also provides information about the MWF distribution and standard error within a structure.

4.4. Mean MWF is more reproducible than median MWF

In the present study, two parameters of the MWF distribution were investigated: the mean and the median. We initially felt that median MWF would be a more effective and robust parameter than mean MWF, as the median is less susceptible to outlier values than the mean. However, median MWF exhibited anomalous behaviour at low MWF values (See Fig. 5), resulting in many zeros in GM structures. The explanation for this behaviour can be deduced from the shape of the histograms in Fig. 4. In many GM structures, close to one half of the voxels gave rise to zero MWF; hence, even though non-zero MWF was present, the median still returned MWF values of zero. This observation, and the fact that the mean square difference for the median MWF on test/retest scans was higher than that for the mean, caused us to drop the median MWF method in favour of the mean MWF approach.

5. Conclusion

Although SNR_{NNLS} for the ROI method was higher, the VBA technique gave rise to similar MWFs as ROI analysis

and was more robust on repeated scans; therefore, we recommend the VBA method over the ROI method for analysing MWF, provided the SNR for an individual voxel is greater than 100.

Acknowledgments

This research was supported by the UBC MS/MRI Research Group, the Natural Sciences and Engineering Research Council (NSERC) and the Multiple Sclerosis Society of Canada. The authors wish to thank all control subjects and the MR technologists at the UBC MRI Research Centre. We also wish to thank Joseph Lee and Eugene Yip for their assistance in developing analysis software and Donna Lang, Yinshan Zhao and Campbell Clark for helpful discussions. S.M.M. was the recipient of an NSERC Undergraduate Scholarship. S.H.K. was the recipient of a Killam Predoctoral Fellowship.

References

[1] MacKay A, Whittall K, Adler J, Li D, Paty D, Graeb D. In vivo visualization of myelin water in brain by magnetic resonance. Magn Reson Med 1994;31(6):673–7.
[2] Menon RS, Allen PS. Application of continuous relaxation time distributions to the fitting of data from model systems and excised tissue. Magn Reson Med 1991;20(2):214–27.
[3] Stewart WA, MacKay AL, Whittall KP, Moore GR, Paty DW. Spin-spin relaxation in experimental allergic encephalomyelitis. Analysis of CPMG data using a non-linear least squares method and linear inverse theory. Magn Reson Med 1993;29(6):767–75.
[4] Whittall KP, MacKay AL, Graeb DA, Nugent RA, Li DK, Paty DW. In vivo measurement of T2 distributions and water contents in normal human brain. Magn Reson Med 1997;37(1):34–43.
[5] Moore GRW, Leung E, MacKay AL, Vavasour IM, Whittall KP, Cover KS, et al. A pathology-MRI study of the short-T2 component in formalin-fixed multiple sclerosis brain. Neurology 2000;55(10): 1506–10.
[6] Webb S, Munro CA, Midha R, Stanisz GJ. Is multicomponent T2 a good measure of myelin content in peripheral nerve? Magn Reson Med 2003;49(4):638–45.
[7] Laule C, Leung E, Lis DK, Traboulsee AL, Paty DW, MacKay AL, et al. Myelin water imaging in multiple sclerosis: quantitative correlations with histopathology. Mult Scler 2006;12(6):747–53.
[8] Laule C, Kozlowski P, Leung E, Li DK, Mackay AL, Moore GR. Myelin water imaging of multiple sclerosis at 7 T: Correlations with histopathology. Neuroimage 2008;40:1575–80.
[9] Flynn SW, Lang DJ, Mackay AL, Goghari V, Vavasour IM, Whittall KP, et al. Abnormalities of myelination in schizophrenia detected in vivo with MRI, and post-mortem with analysis of oligodendrocyte proteins. Mol Psychiatry 2003;8(9):811–20.
[10] Oakden W, Lobaugh NJ, Black S, Stanisz GJ. Quantitative T2 Relaxation of White Matter Hyperintensities in Probable Alzheimer Patients. 2007. p 2146.
[11] Oh J, Han ET, Pelletier D, Nelson SJ. Measurement of in vivo multi-component T2 relaxation times for brain tissue using multi-slice T2 prep at 1.5 and 3 T. Magn Reson Imaging 2006;24(1):33–43 Electronic Publication 19 Dec 2005.
[12] Sirrs SM, Laule C, Maedler B, Brief EE, Tahir SA, Bishop C, et al. Normal appearing white matter in subjects with phenylketonuria: water content, myelin water fraction, and metabolite concentrations. Radiology 2007;242(1):236–43.
[13] Tozer DJ, Davies GR, Altmann DR, Miller DH, Tofts PS. Correlation of apparent myelin measures obtained in multiple sclerosis patients and controls from magnetization transfer and multicompartmental T2 analysis. Magn Reson Med 2005;53(6):1415–22.
[14] Vidarsson L, Conolly SM, Lim KO, Gold GE, Pauly JM. Echo time optimization for linear combination myelin imaging. Magn Reson Med 2005;53(2):398–407.
[15] Wu Y, Alexander AL, Fleming JO, Duncan ID, Field AS. Myelin water fraction in human cervical spinal cord in vivo. J Comput Assist Tomogr 2006;30(2):304–6.
[16] Du YP, Chu R, Hwang D, Brown MS, Kleinschmidt-DeMasters BK, Singel D, et al. Fast multislice mapping of the myelin water fraction using multicompartment analysis of T2∗ decay at 3T: a preliminary postmortem study. Magn Reson Med 2007;58(5):865–70.
[17] Poon CS, Henkelman RM. Practical T2 quantitation for clinical applications. J Magn Reson Imaging 1992;2(5):541–53.
[18] Foltz WD, Al-Kwifi O, Sussman MS, Stainsby JA, Wright GA. Optimized spiral imaging for measurement of myocardial T2 relaxation. Magn Reson Med 2003;49(6):1089–97.
[19] Graham SJ, Stanchev PL, Bronskill MJ. Criteria for analysis of multicomponent tissue T2 relaxation data. Magn Reson Med 1996;35 (3):370–8.
[20] Mädler B, MacKay AL. In-vivo 3D Multi-component T2-Relaxation Measurements for Quantitative Myelin Imaging at 3T; 2006. p. 2112. Seattle, USA.
[21] Armspach JP, Gounot D, Rumbach L, Chambron J. In vivo determination of multiexponential T2 relaxation in the brain of patients with multiple sclerosis. Magn Reson Imaging 1991;9 (1):107–13.
[22] Papanikolaou N, Maniatis V, Pappas J, Roussakis A, Efthimiadou R, Andreou J. Biexponential T2 relaxation time analysis of the brain: correlation with magnetization transfer ratio. Invest Radiol 2002;37 (7):363–7.
[23] Stanisz GJ, Henkelman RM. Diffusional anisotropy of T2 components in bovine optic nerve. Magn Reson Med 1998;40(3):405–10.
[24] Moody JB, Xia Y. Analysis of multi-exponential relaxation data with very short components using linear regularization. J Magn Reson 2004;167(1):36–41.
[25] Beaulieu C, Fenrich FR, Allen PS. Multicomponent water proton transverse relaxation and T2-discriminated water diffusion in myelinated and nonmyelinated nerve. Magn Reson Imaging 1998;16 (10):1201–10.
[26] Fenrich FR, Beaulieu C, Allen PS. Relaxation times and microstructures. NMR Biomed 2001;14(2):133–9.
[27] Gareau PJ, Rutt BK, Karlik SJ, Mitchell JR. Magnetization transfer and multicomponent T2 relaxation measurements with histopathologic correlation in an experimental model of MS. J Magn Reson Imaging 2000;11(6):586–95.
[28] Whittall KP, MacKay AL. Quantitative interpretation of NMR relaxation data. J Magn Reson 1989;84:134–52.
[29] Kolind SH, Maedler B, Li DKB, MacKay AL. Imaging myelin in vivo; comparison of the T2 distribution at 1.5T and 3.0T; 2006. p. 3121. Seattle, USA.
[30] Pluim JP, Maintz JB, Viergever MA. Mutual-information-based registration of medical images: a survey. IEEE Trans Med Imaging 2003;22(8):986–1004.
[31] Lawson CL, Hanson RJ. Solving Least Squares Problems. Englewood Cliffs (N.J.): Prentice-Hall; 1974.
[32] Skinner MG, Kolind SH, Mackay AL. The effect of varying echo spacing within a multiecho acquisition: better characterization of long T(2) components. Magn Reson Imaging 2007;25(6):834–9.
[33] Bland JM, Altman DG. Statistical methods for assessing agreement between two methods of clinical measurement. Lancet 1986;1 (8476):307–10.
[34] Whitaker KJ, Kolind SH, Mackay AL, Clark CM. Quantifying development: Investigating highly myelinated voxels in preadolescent corpus callosum. Neuroimage 2008.

[35] Galbraith SM, Lodge MA, Taylor NJ, Rustin GJ, Bentzen S, Stirling JJ, et al. Reproducibility of dynamic contrast-enhanced MRI in human muscle and tumours: comparison of quantitative and semi-quantitative analysis. NMR Biomed 2002;15(2):132–42.

[36] Figueiredo PM, Clare S, Jezzard P. Quantitative perfusion measurements using pulsed arterial spin labeling: effects of large region-of-interest analysis. J Magn Reson Imaging 2005;21(6): 676–82.

[37] Vold RL, Vold RR, Simon HE. Errors in measurements of transverse relaxation rates. J Magn Reson 1973;11:283–98.

[38] Does MD, Snyder RE. T2 relaxation of peripheral nerve measured in vivo. Magn Reson Imaging 1995;13(4):575–80.